PRACTICAL EXAMPLE OF THE SUPERVISED VICARIOUS CALIBRATION (SVC) METHOD – VALCALHYP AIRBORNE HYPERSPECTRAL CAMPAIGN UNDER EUFAR

Anna Brook[1], and Eyal Ben-Dor[2]

1. Remote Sensing Laboratory, Center for Spatial Analysis Research (UHCSISR), Department of Social Sciences, University of Haifa, Mount Carmel, Israel; abrook(at)geo.haifa.ac.il
2. Remote Sensing Laboratory, Department of Geography and Human Environment, Tel-Aviv University, Ramat Aviv, Israel; bendor(at)post.tau.ac.il

ABSTRACT

A novel reflectance-based approach for radiometric calibration and atmospheric correction of airborne hyperspectral (HRS) data, supervised vicarious calibration (SVC), was proposed by Brook and Ben-Dor in 2011. The present study aimed to validate the SVC method using simultaneously operated several different airborne HRS sensors that acquired data above several selected sites. The general goal is thus to apply a cross-calibration approach to examine the capability and stability of the SVC method. In the current study three sensors were involved in an airborne campaign mission supported by EUFAR under a project entitled ValCalHyp. The AISA-Dual (operated by NERC), AHS and CASI (operated by INTA) acquired data over several selected sites in the south of France (Salon de Province, Marseille, Avignon and Montpellier) on 28 October 2010 between 13:00 and 16:00 UTC.

INTRODUCTION

General

Hyperspectral remote sensing (HRS) has become a common tool for environmental and geosciences applications. The increasing spatial and spectral resolutions and accuracy, together with the broad information of airborne HRS image data provide new possibilities for quantitative surface recognition and classification in these applications. Recently more and more HSRS sensors entering the field of remote sensing (1) and more users are exposed to this promising technology. Furthermore, data fusion between many sensors is widely used in environmental applications. Data fusion techniques combine data from multiple sensors, and related information from associated databases, to achieve improved accuracies and more detailed information than could be achieved by the use of a single sensor alone. While, a single-source information support proven preprocessing and processing techniques, the integrated multi-sensors data provide complementary information of the scene by applying dedicated methods and techniques for HRS data analysis, such as image enhancement, spectral unmixing and pattern recognition. If merged properly, fusion of data may lead to a detailed and consistent scene description. Generally, fusion of multi-sensor data provides obvious advantages over single-source data, such as the statistical advantage and higher overall accuracy.

The HSRS information at all configurations (single- or multi- sensors) requires the extraction of reliable physical inherent units as reflectance (2). The key factor in the extraction of quantitative information from HRS images is based on spectral reflectance is accurate at-sensor radiometric information, which depends on the illumination geometry and on the reflectance characteristics of the observed surface. Therefore, as part of data correction and rectification towards achieving actual radiometric values, and consequently reliable reflectance information, both radiometric and atmospheric corrections have to be performed for each sensor independently (3). However, the success of multi-sensor data fusion relies mainly on the original quality of the input data, while

DOI: 10.12760/01-2014-2-01

integration between accurate and inaccurate or data, especially if the uncertainties of the data are unknown, might lead to wrong and unacceptable results.

The SVC approach

The main assumption of the supervised vicarious calibration (SVC) method (4) is that radiometric and spectral performances and stability of all HRS sensors are varying in time and space, therefore the periodical calibration information, such as laboratory calibration, might not hold for every campaign. Thus, a method to assess the overall accuracy of at-sensor radiance response and its stability alongside with correcting the possible radiance drifts are crucial, and suggested by the SVC method. The basis of the SVC method relies on in-situ spectral measurements of a selected test site on the airplane's trajectory that is covered by artificial agricultural black polyethylene nets in various densities. These targets are set up on the ground close in time to the beginning of the airborne campaign, and are use to radiometrically recalibrate the HRS sensor, in case it is necessary. The different densities of the nets combined with any bright background afford full coverage of the HRS sensor's dynamic range

The current project

In the presented project, the SVC method was validated at a selected European site set near Montpellier on the parking lot next to a coastline. This site provided a wide flat region mainly covered by very bright sand dune. During the flight campaign two scenarios for cross-calibration were performed: the ideal scenario, when all sensors share the same geometry (in terms of flight heading) and the coincident acquisitions (sensing the same area with the same geometry), and the less ideal (more realistic) scenario, when the sensors does not share the same geometry but keep the coincident acquisitions, or when the sensors holds different geometry and different acquisitions. This project studies cross-calibration results for all the above-mentioned scenarios and compared the results between AISA-Dual (from NERC), AHS and CASI sensors (from INTA). A brief overview of the sensors used for the cross-calibration is given and the SVC test site is discussed. The results of the SVC method were examined by comparing the ground-truth spectra of several selected validation targets with the imagery spectra corrected by the suggested method for the three HRS sensors.

METHODS

Data acquisition

The AISA-DUAL is an airborne imaging spectrometer designed and built by SpecIm Ltd. This instrument was operated by NERC (Natural Environment Research Council, UK) team on board of Do228 aircraft at an altitude of 3.3 km. It simultaneously acquires images in varying configurations of contiguous spectral bands (with up to 190 bands between 400-970 nm and 244 bands between 970-2.450 nm), covering the 400-2.450 nm spectral region using the dual system of the AISA-EAGLE device for the VIS-NIR region and the AISA-HAWK device for the SWIR region. A standard AISA-DUAL dataset is a 3D data cube in the non-earth coordinate system (not geo-rectified). It has 286 pixels in the cross-track direction and hundreds of pixels in the along-track direction

The AHS is an airborne imaging spectrometer with 80 bands built by Sensytech Inc. (currently Argon ST, and formerly Daedalus Inc.) and purchased by INTA (ES) on 2003. This sensor was operated by INTA (ES) team on board of CASA C-212 aircraft at an altitude of 2.1 km. In the VIS/NIR range, 19 broad bands (~30 nm) are covering the 430-1.000 nm spectral region. In the SWIR range is a set of continuous, fairly narrow bands (~13 nm) between 2.000 and 2.500 nm. In the MIR and TIR ranges, high spectral resolution (30 to 50 nm) is covering the 3 to 5 μm and 8 to 13 μm atmospheric windows.

The CASI is an airborne imaging spectrometer in VNIR region with 1500 pixels in the cross-track direction and hundreds of pixels in the along-track direction, allowing imaging a vast area with a single pass. This instrument was operated by INTA (ES) team on board of CASA C-212 together with the AHS system. It simultaneously acquires images in varying configurations of contiguous

spectral bands (with up to 670 bands) covering the 380-1.050 nm spectral region with spatial resolution of 0.5 m^2.

Ground sites of interest

The SVC targets were rolled up two hours before the over flight took place as seen in Figure 1.

Figure 1: The ground calibration site of the supervised vicarious calibration (SVC) method set near Montpellier, France on the parking lot next to a coastline (image source Google Earth).

The ground spectra of the SVC targets were measured with the portable field spectrometer ASD Field SpecPRO (Analytical Spectral Device, Boulder, CO) which consists of 2.151 wavelengths ranging between 350 and 2.500 nm, with bandwidths of 2 nm in the VNIR region (350-1.050 nm) and 10 nm in SWIR region (1.050-2.500 nm), and wavelength accuracy of ±1 nm/±0.1 nm. Each ground target (the nets, the background surface and the targets to be validated) was measured by averaging 40 spectra of both radiance and reflectance values during the overpass. The reflectance mode was calibrated against a Spectralon® white reference panel. The optimization procedure was programmed to work in both radiance and reflectance modes, averaging 40 replications per measured spectrum. Each target was measured systematically by collecting about 40 points along the net's long axis to the direction of the flight. All points in a designed matrix were about 3 m distant from each other and the spectral measurement was taken from 1 m height with a bare-optics of a 24° field of view (FOV) (about 60 cm^2 footprint) with spectral error (standard deviation)

Two addition thematic area sites were selected in Southern France and acquired during the same flight. First is an urban region in Salon-de-Provence (Figure 2) and the second is a maritime region in the port of Marseille (Figure 3).

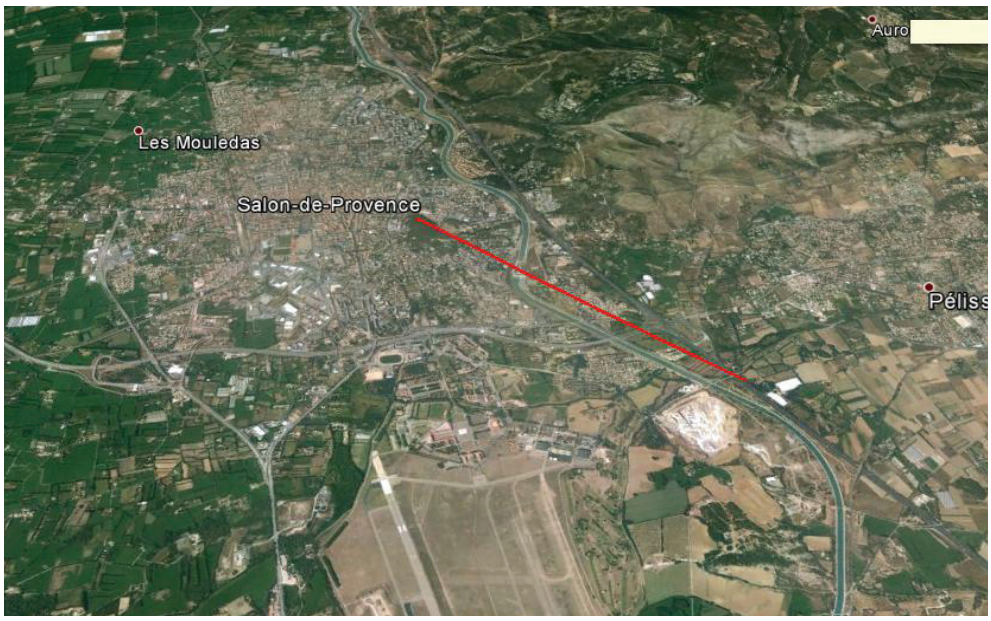

Figure 2: Urban region of interest in Salon-de-Provence (image source: Google Earth).

Figure 3: Maritime region of interest in Marseille (image source: Google Earth).

Calibration action

To avoid any illumination gradients across-track, the flight lines are usually headed towards the sun. In the reported campaign, the SVC site was covered by six flight lines in a cross-shape pattern with two parallel but overlap (~50%) lines (producing four flight lines) with headings of 289 and 109 degrees and one line (producing two flight lines) with headings of 19 and 199 degrees respectively. The thematic area sites, at Salon-de-Provence and the port of Marseille, were

acquired by flight lines with headings of 349 and 226 degrees respectively. The different geometry of the net targets was in order to evaluate whether the direction of the net and the direction of the thematic flight line should keep the same heading.

During the flight campaign two SVC scenarios were performed: 1) the ideal scenario, when all sensors share the same geometry (in terms of flight heading) and the coincident acquisitions (sensing the same area with the same geometry), and 2) the less ideal (more realistic) scenario, when the sensors does not share the same geometry but keep the coincident acquisitions, or when the sensors holds different geometry and different acquisitions. The calibration coefficients, *L*(*gain*) and *L*(*offset*), were evaluated for each scenario and applied at the following order: for the ideal scenario (sc_#1), the two parallel and overlap flight lines above the SVC site were used, when one flight line was submitted to calibration and another flight line was referred as validation (or thematic area site) in the SVC vicinity. The less ideal scenario were subdivided into two categories: the first group (sc_#2) illustrated scenario where calibration and validation flight lines did not share the same geometry but preserved the coincident acquisitions by applying the SVC calibration coefficients (flight line with 289 degree heading) on the cross-shape pattern flight lines coefficients (flight line with 19 degree heading), the second group illustrated scenario (sc_#3) where calibration and validation flight lines kept the same geometry but did not share the coincident acquisitions by applying the SVC calibration coefficients of the flight line with 289 degrees heading on the validation flight line with 226 degree heading above the port of Marseille. The last examination (sc_#4) was performed on the Salon-de-Provence flight line with headings of 349 degree applying the SVC calibration coefficients of the flight line with 199 degrees heading.

RESULTS

The full correction sequence extracts four factors from the four stages (F1, F2, F3 and F4), that are saved and then later applied to all images from the same campaign, considering all that the sensor drift obtained over the SVC location stay constant for the current operation. Further, two basic index to judge the radiometric performances radiance-to-reflectance ration (*Rad*/*Ref*) and Radiance-to-Reflectance Difference Factor (*RRDF*) were also used (see more details on that factors and indices in (3)). Table 1 demonstrates the *F* test, *T* test and Pearson's correlation coefficients for the *Rad*/*Ref* and the *RRDF* indicators of the original AISA-DUAL, AHS and CASI radiance, and coarse-corrected (F1) and fine-corrected (F2) radiance of the SVC nets targets (3).

The reflectance accuracy of the individual data set (different scenario and cross-calibration sets of coefficients) might vary based on an overall accuracy of the calibration procedure. Therefore, to compare the results of all possible cross-calibration scenarios (ideal and less ideal) all possible combinations of the SVC method (emphasizing the normalization of the albedo sequence (F1) and radiometric calibration using the SVC net reflectance (F2) to obtain calibration coefficients) were examined and illustrated in Figure 4.

Radiometric error is an uncorrelated and normally distributed random variable, which considered to be "combined standard uncertainty level" (5) of type A error (random uncertainties determined by statistical analysis) and of type B error (systematic error). Both can be result of deteriorating the detectors as well as different sources of noises obtained from the sensor surroundings. In HRS domain, a type A error is linked to sensor noise and type B error might express radiometric calibration error (5). In this study, type B errors are dominate as the main components to the global uncertainty level and relative radiometric uncertainty level, represented by 95% confidence interval for random error (from normal distribution) or sensitivity coefficient. The sensitivity coefficient defined as the ratio of the relative standard deviation (calculated for the full spectral region) of an original (input) at-sensor radiance to the ratio the relative standard deviation of the corrected at-sensor radiance (product of F2 stage). Table 2 and Figure 5 show the relative uncertainty level of the retrieved radiometric coefficient for AISA-Dual according to all examined scenarios (sc_#1,2,3,4) calculated on three selected ground-truth validation targets: tar1 – soil path, tar2 – asphalt, tar3 – concrete.

Table 1: Descriptive statistics of Rad/Ref and RRDF indicators for an original AISA-DUAL, AHS and CASI radiance, and coarse-corrected (F1) and fine-corrected (F2) radiance of the SVC nets targets.

Descriptive Statistics	AISA-DUAL (Original) Radiance				F1 Radiance				F2 Radiance			
	Rad/Ref			RRDF	Rad/Ref			RRDF	Rad/Ref			RRDF
	VIS	NIR	SWIR		VIS	NIR	SWIR		VIS	NIR	SWIR	
N	4	4	4	3	4	4	4	3	4	4	4	3
F test's Sig.	0.3	0.1	0.1	0.5	0.03*	0.03*	0.02*	0.04*	0.005*	0.005*	0.005*	0.005*
T test's Sig.	0.314	0.12	0.1	0.53	0.04*	0.04*	0.04*	0.07	0.005*	0.005*	0.005*	0.005*
x mean	0	0	0	NA	0	0	0	NA	0	0	0	0
y mean	0.31	0.1	0	NA	0	0	0	NA	0	0	0	0
Σxy	NA	NA	NA	NA	46	46	42	NA	68	63	67	49
R	NA	NA	NA	NA	0.53	0.6	0.62	NA	0.99	0.99	0.99	0.98
Sig. (2-tailed)	NA	NA	NA	NA	0.01*	0.01*	0.01*	NA	0.01*	0.01*	0.01*	0.01*

Descriptive Statistics	AHS (Original) Radiance				F1 Radiance				F2 Radiance			
	Rad/Ref			RRDF	Rad/Ref			RRDF	Rad/Ref			RRDF
	VIS	NIR	SWIR		VIS	NIR	SWIR		VIS	NIR	SWIR	
N	4	4	4	3	4	4	4	3	4	4	4	3
F test's Sig.	0.3	0.1	0.08	0.5	0.04*	0.03*	0.04*	0.04*	0.005*	0.005*	0.005*	0.004*
T test's Sig.	0.2	0.15	0.1	0.5	0.05*	0.05*	0.05*	0.07	0.01*	0.01*	0.01*	0.01*
x mean	0	0	0	NA	0	0	0	NA	0	0	0	0
y mean	0.8	0.1	0	NA	0	0	0	NA	0	0	0	0
Σxy	NA	NA	NA	NA	47	44	40	NA	64	59	61	49
R	NA	NA	NA	NA	0.83	0.8	0.76	NA	0.98	0.98	0.98	0.97
Sig. (2-tailed)	NA	NA	NA	NA	0.01*	0.01*	0.01*	NA	0.01*	0.01*	0.01*	0.01*

Descriptive Statistics	CASI (Original) Radiance		F1 Radiance		F2 Radiance	
	Rad/Ref	RRDF	Rad/Ref	RRDF	Rad/Ref	RRDF
	VIS		VIS		VIS	
N	4	3	4	3	4	3
F test's Sig.	0.5	0.3	0.04*	0.04*	0.005*	0.004*
T test's Sig.	0.3	0.1	0.05*	0.07	0.01*	0.01*
x mean	0	NA	0	NA	0	0
y mean	0.8	NA	0	NA	0	0
Σxy	NA	NA	47	NA	64	49
R	NA	NA	0.83	NA	0.98	0.97
Sig. (2-tailed)	NA	NA	0.01*	NA	0.01*	0.01*

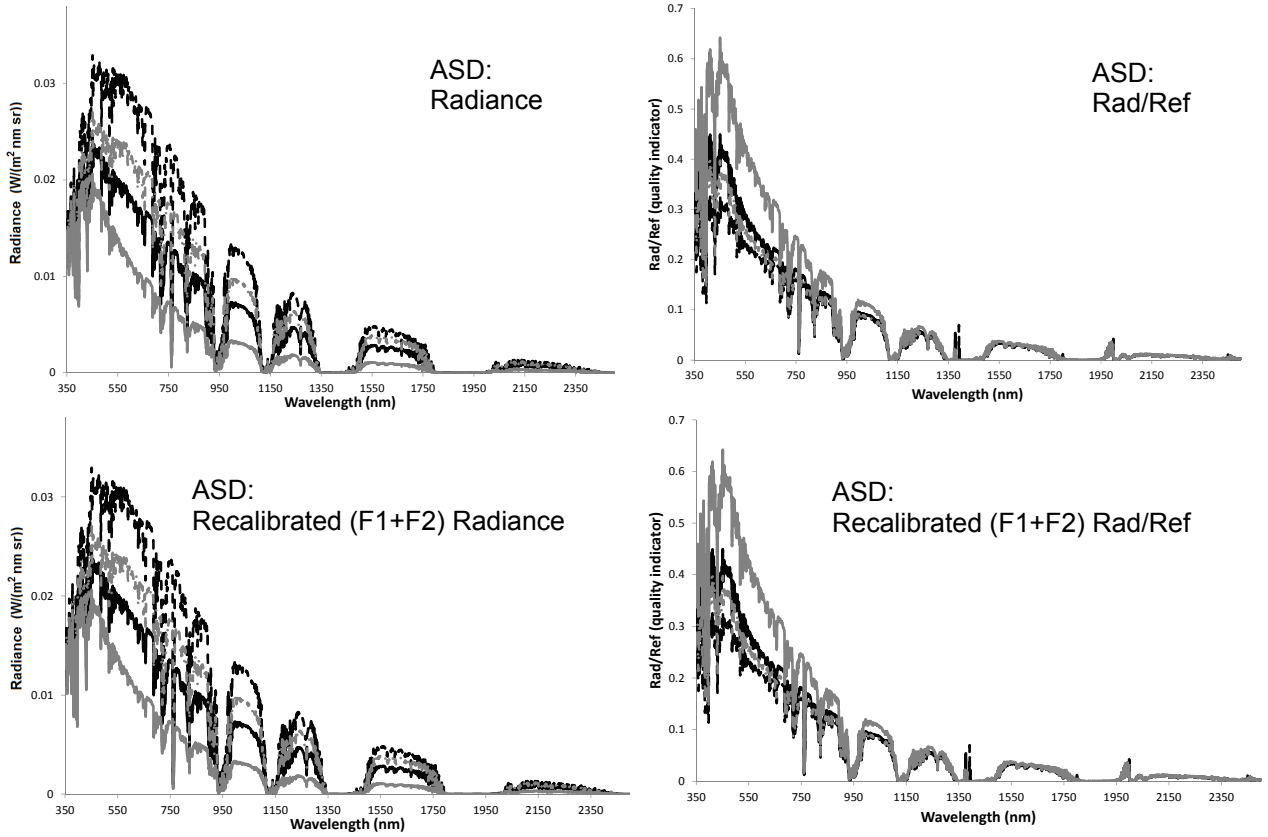

Figure 4a: The original radiance and the corresponding Rad/Ref index, the recalibrated (F1 and F2 SVC stages) radiance and the corresponding Rad/Ref index of the ASD sensor.

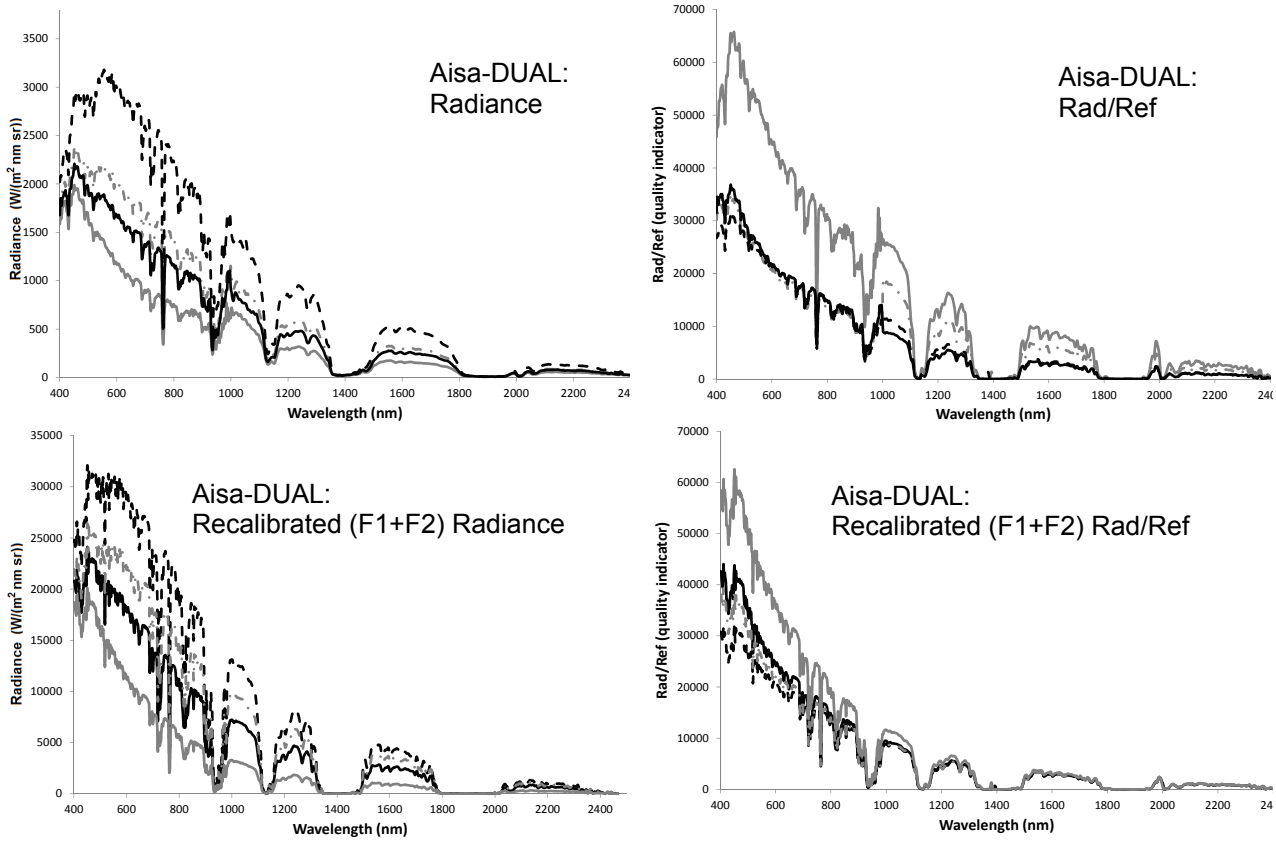

Figure 4b: The original radiance and the corresponding Rad/Ref index, the recalibrated (F1 and F2 SVC stages) radiance and the corresponding Rad/Ref index of the Aisa-DUAL sensor.

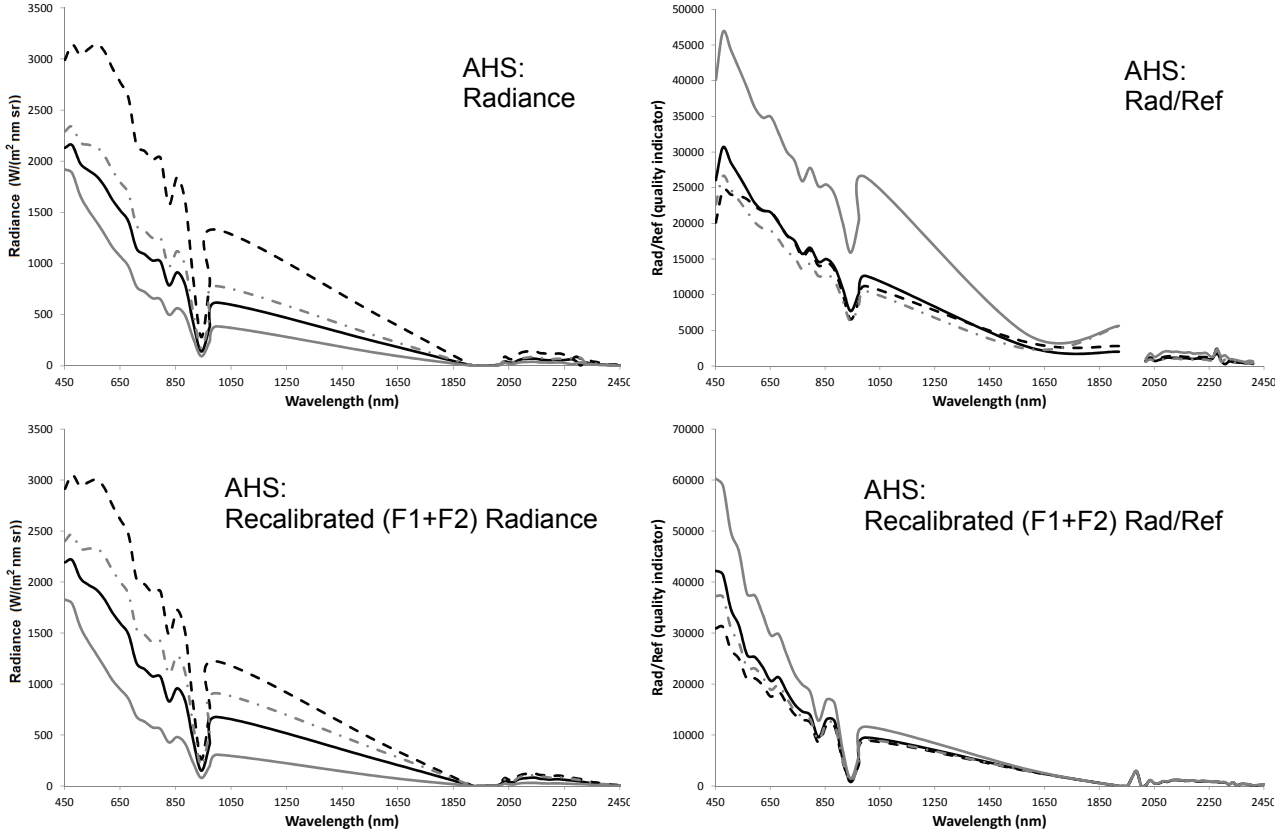

Figure 4c: The original radiance and the corresponding Rad/Ref index, the recalibrated (F1 and F2 SVC stages) radiance and the corresponding Rad/Ref index of the AHS sensor.

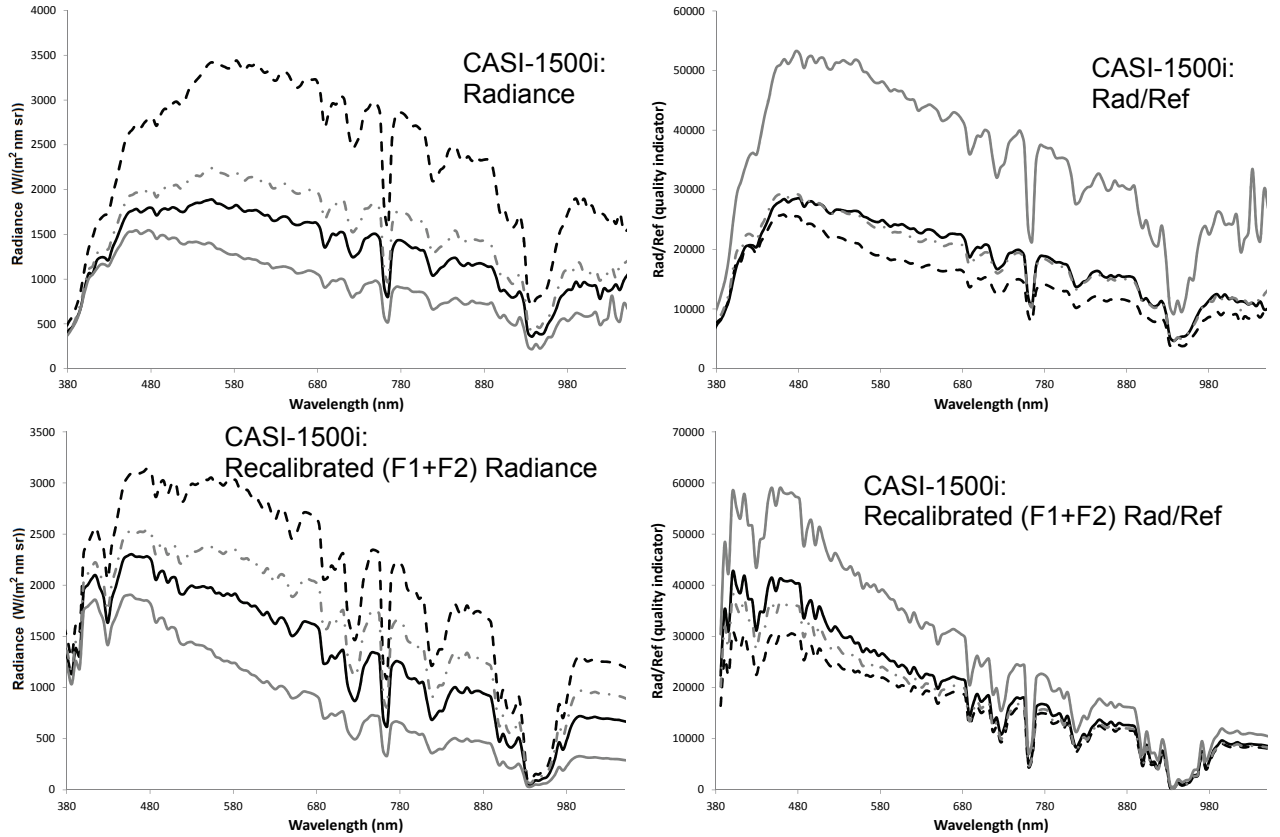

Figure 4d: The original radiance and the corresponding Rad/Ref index, the recalibrated (F1 and F2 SVC stages) radiance and the corresponding Rad/Ref index of the CASI-1500i sensor.

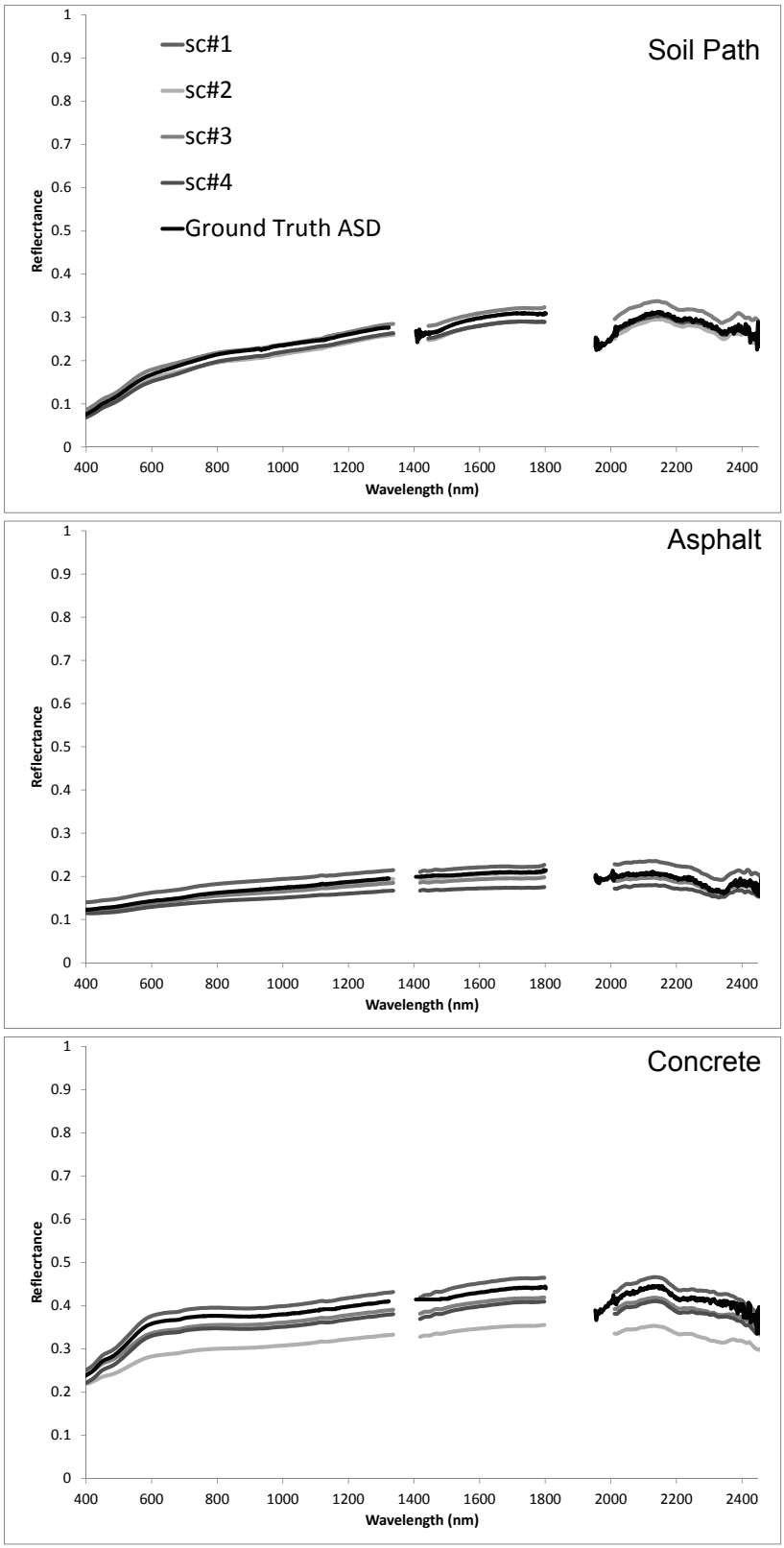

Figure 5: The spectra of three different targets as obtained at each sensors after applying the SVC and the ground truth spectra (measured by the ASD field spectrometer).

The complete protocol on the practical execution of the cross-calibrated SVC results is further discussed together with the possible limitations of the proposed method. It is therefore crucial to compare the thematic results of each of the procedure used to derive the reflectance information from the corrected radiance data (Figure 6). We therefore present the thematic mapping accuracy

of the atmospherically corrected images over well-known areas. For the interpretation of the obtained reflectance data, we applied the water quality index (WQI) on the thematic maritime site (6). While, the water quality is defined as the chemical, physical and biological characteristics of water bodies, the WQI classifies water quality in a representative scale from 100 to 0 (as good, moderated, mean, warning and poor qualities).

Table 2: The uncertainty level of the retrieved radiometric coefficient.

Sensor/ Correction scenario Targets	sc_#1			sc_#2			sc_#3			sc_#4		
	Tar1	Tar2	Tar3	Tar1	Tar2	Tar3	Tar1	Tar2	Tar3	Tar1	Tar2	Tar3
AISA-Dual	0.2	0.01	0.01	1.9	1.5	1.5	1.7	1.3	1.2	2.1	1.9	1.7
AHS	0.4	0.1	0.01	3.5	2.1	1.8	3.1	2.5	2.1	3.9	3.6	3.5
CASI	1.0	0.6	0.1	4.1	2.8	2.2	3.1	4.3	1.5	4.5	3.9	3.2

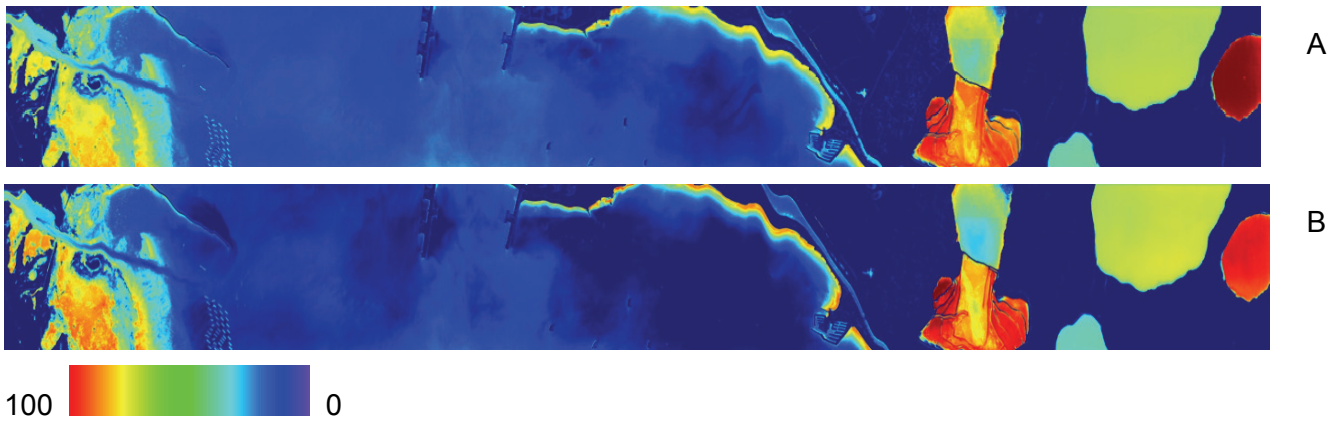

Figure 6: The results of the applied index to AISA-Dual data show the spatial distribution of water quality in the selected region for calibration ideal (sc_#1) and less ideal (sc_#4) scenarios.

The cross-calibration results for several predefined flight configurations compared the results between multi-sensor information acquired the above-mentioned airborne sensors. In Table 3 the quantitative evaluation involved calculating two indicators, ASDS (applicable on all HRS sensors) (7) and ASDS-s (applicable on AISA-Dual sensor) (3), for all scenarios.

Table 3: The ASDS and the ASDS-(S) indicators for all scenarios.

Sensor/ Correction scenario Targets	sc_#1			sc_#2			sc_#3			sc_#4		
	Tar1	Tar2	Tar3	Tar1	Tar2	Tar3	Tar1	Tar2	Tar3	Tar1	Tar2	Tar3
AISA-Dual	0.005 **0.001**	0.0014 **0.0001**	0.0011 **0.0001**	0.009 **0.005**	0.005 **0.001**	0.006 **0.001**	0.017 **0.006**	0.002 **0.005**	0.002 **0.001**	0.22 **0.07**	0.13 **0.03**	0.14 **0.05**
AHS	0.08	0.0018	0.0007	0.1	0.05	0.05	0.08	0.001	0.001	0.38	0.21	0.28
CASI	0.05	0.008	0.005	0.09	0.05	0.05	0.07	0.005	0.001	0.42	0.27	0.32

The results of this project confirmed that the SVC approach performed identically well for the selected HRS sensors in both ideal and less ideal scenarios. In fact, the good agreement shown between the ground-truth validation spectra and the imagery spectra (Table 3), suggests that the

SVC approach is feasible for any of the selected HRS sensors and it is strongly recommended for the future utilization.

CONCLUSIONS

The SVC method proposed herein was allied on multi-source HRS simultaneously acquired data sets in order to obtain favourable reflectance extraction and realistic thematic products. Three airborne HRS sensors: Aisa-DUAL, AHS and CASI-1500i were subjected to this method in different flight heading and scanning configurations, introducing two scenarios (ideal scenario -where all sensors shared the same geometry over the SVC and AOI areas and 2) the non-ideal scenario - where the sensors does not share the same geometry over the SVC and AOI areas). The current sensor could not provide reliable reflectance information from its radiance values using ordinary correction techniques (e.g. EL or atmospheric model). The suggested SVC approach can rectify the data, producing near real physical units that can then be further used to spectrally analyse and produce thematic maps. For the current SVC approach, we suggest using artificial ground targets that are easy to maintain, transport and measure, located near the airfield. The main benefit of the suggested targets is that they are made of the same material with different mixing rates that end up covering the entire dynamic range of the sensor. The two immediate indicators to assess the quality of the data (Rad/Ref and RRDF) based on the reflectance and radiance of the net targets on the ground allowed to inspect the quality data rapidly before flying long distances. The simplicity of the SVC calibration site and the ability to provide quality indicators information rapidly suggest that the SVC method is practical, feasible and promising for many similar cases.

ACKNOWLEDGEMENTS

The authors wish to thank European Facility for Airborne Research EUFAR (www.eufar.net) for funding of the flight campaign (Transnational Access Project „ValCalHyp“) and thank INTA’s crew members (AHS and CASI-1200i sensors onboard the CASA platform) and NERC's crew members (AisaDUAL on DORNIER 228 platform) for the airborne data acquisition.

REFERENCES

1 Eyal Ben-Dor, 2013: Hyperspectral remote sensing. In: Airborne Measurements for Environmental Research: Principles and Methods, edited by M Wendisch & J-L Brenguier, Chapter 8 (Wiley VCH) 640 pp.

2 Goetz, A F H, G Vane, J Solomon & B N Rock, 1985. Imaging spectrometry for Earth remote sensing, Science, 228: 1147-1153

3 Brook A, E Ben-Dor & R Richter, 2011. Modeling and monitoring urban built environment via multi-source integrated and fused remote sensing data. International Journal of Image and Data Fusion, 3: 1-31

4 Brook A & E Ben-Dor, 2011. Supervised vicarious calibration (SVC) of hyperspectral remote-sensing data. Remote Sensing of Environment, 115 (6): 1543-1555

5 Nieke J, K Itten, M Koen, P Gege, F Dell’Endice, A Hueni, G Ulbrich & R Meynart, 2008. Supporting Facilities for the Airborne Imaging Spectrometer APEX, 4 pp. In: IEEE International Geosciences and Remote Sensing Symposium (IGARSS) (July 6-11, Boston, MA)

6 Abassi S A, 1999. Water quality indices: state -of-the art. Journal IPHE, 21: 22-25

7 Ben-Dor E, B Kindel & A F H Goetz, 2004. Quality assessment of the empirical line method to recover surface reflectance information using synthetic AVIRIS data. Remote Sensing of Environment, 90: 389-404